NSF Grant # 0826276
NSF PROGRAM NAME: Dynamical Systems

The Effects of Asymmetry on the Dynamics of Nanowires

Molly R. Nelis, Lin Yu, Saeed Mohammadi[Co-PI], **Arvind Raman**[Co-PI], **Jeffrey F. Rhoads**[PI]
Birck Nanotechnology Center, Purdue University

Abstract: This work investigates the effects of asymmetric cross-sectional geometry on the resonant response of silicon nanowires. The work demonstrates that dimensional variances of less than 2% qualitatively alter a nanosystem's near-resonant response, yielding a non-Lorentzian frequency response structure, which is a direct consequence of resonant mode splitting. Experimental results show that this effect is independent of material properties and device boundary conditions, and can be easily modeled using a two-degree-of-freedom system. Proper understanding of this phenomenon is believed to be essential in the characterization of the dynamic response of resonant nanotube and nanowire systems, and thus the predictive design of such devices.

1. Introduction: Resonant nanowire systems have demonstrated utility in applications ranging from radio frequency (RF) filtering and mass sensing to quantum-level detection [1, 2]. The functionality of these devices is commonly founded upon the single-peak, Lorentzian frequency response structure that is associated with a predominately single-degree-of-freedom resonator. Nanofabrication process variability results in structures with asymmetric cross-sectional geometries. Silicon nanowires, for example, commonly feature irregular hexagonal cross sections [3, 4], as shown in Fig. 1. Small dimensional variances and asymmetries (often <2% of the nominal dimension) qualitatively alter a nanosystem's near-resonant response, yielding a multi-peak, non-Lorentzian frequency response structure (provided that the ambient pressure is sufficiently low enough that the peaks do not overlap – see Fig. 2). This mode splitting effect was previously observed by Gil-Santos and collaborators [5]. Given the endemic nature of this response feature in all resonant nanowire devices, particular care must be taken to account for this effect in the course of predictive design.

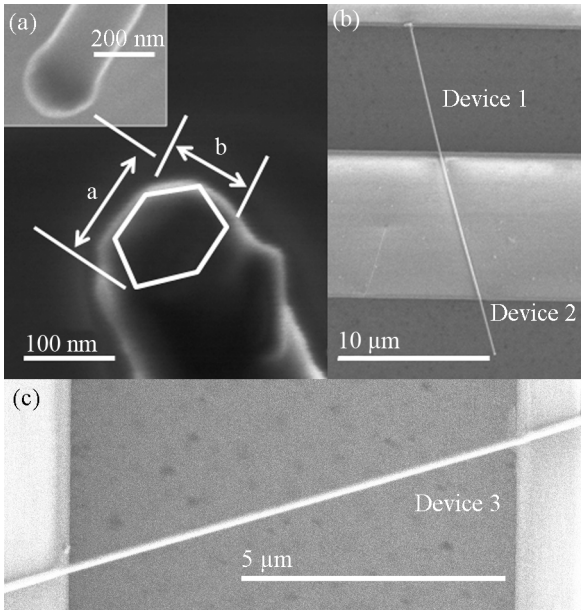

Figure 1: (a) Scanning electron micrograph (SEM) of a silicon nanowire's cross-section. Note that the inset highlights the catalyst remaining on the end of an intact wire following fabrication. (b) SEM of two typical devices. Note that the lighter regions here are the SU-8 grating, while the darker regions are the silicon substrate. Device 1 features an effective fixed-pinned boundary condition, while Device 2 is cantilevered. (c) SEM of Device 3, a silicon nanowire with fixed-fixed boundary conditions.

2. Model: Generally speaking, resonant mode splitting does not occur in devices with circular or regular hexagonal cross sections, as the orthogonal modes of vibration, transverse to the cross-sectional plane, associated with each resonance occur at identical frequencies in these systems. In the presence of cross-sectional irregularity, each of these resonance peaks split, yielding nearly-orthogonal modes with distinct natural frequencies. This effect also occurs in elliptical cross sections, as observed by Garrett [6].

By using a model that parameterizes an irregular

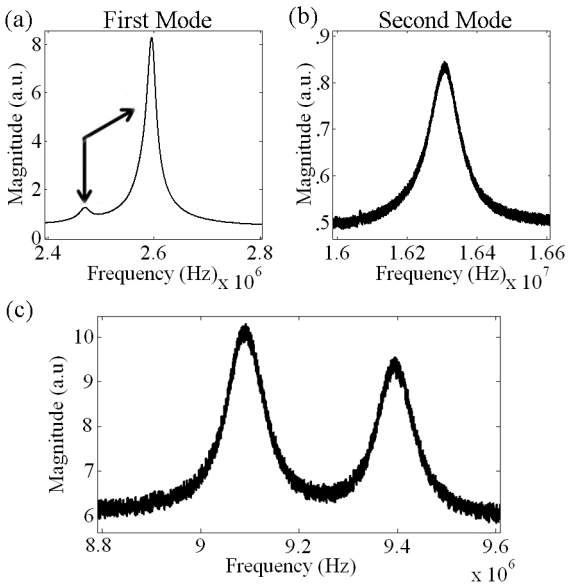

Figure 2: The experimental frequency response of silicon nanowires excited by thermal noise, as measured at room temperature in a 2 mTorr environment. Insets (a) and (b) highlight the response of a cantilevered nanowire near its first and second modes of vibration. Note that inset (a) shows resonant mode splitting, while inset (b) does not. The absence of resonant mode splitting near the second mode of oscillation may be due to the resonant response being below the thermomechanical noise floor. Inset (c) highlights the response of a fixed-fixed nanowire near its first mode of vibration. Appreciable mode splitting is evident.

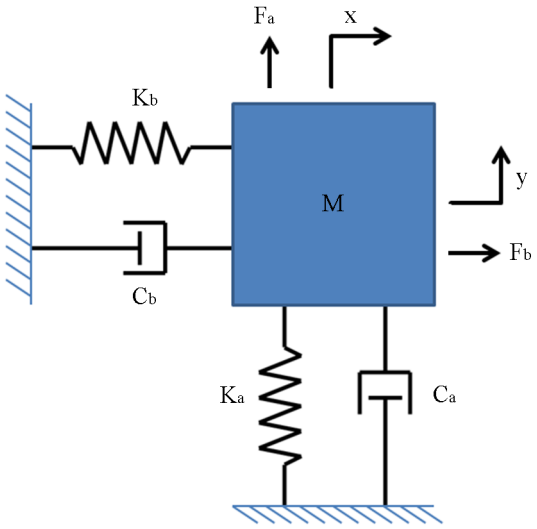

Figure 3: A schematic of the two-degree-of-freedom model for a mistuned resonator.

hexagon by the largest vertex-to-vertex distance (a) and perpendicular width (b), see Fig. 1, the frequencies of a given nanowire's split modes can be represented by a beam in lateral vibration with undamped natural frequencies (in Hz) given by $f_{a,b}$:

$$f_{a,b} = \frac{\beta^2}{2\pi}\sqrt{\frac{EI_{a,b}}{\rho A}} \tag{1}$$

Here, β is a boundary condition dependent factor, EI represents the system's flexural rigidity, ρ represents the system's mass density, A defines the resonator's cross-sectional area, and I_a and I_b delineate the device's cross-sectional moments of inertia. The latter parameters are defined according to:

$$A = \frac{3ab}{4} \tag{2}$$

$$I_a = \frac{5ab^3}{96} \tag{3}$$

$$I_b = \frac{5a^3b}{128} \tag{4}$$

Note that when a and b are parameterized such that the hexagon is regular, the values of I_a and I_b are identical.

The aforementioned split in resonant frequencies and associated modes can be quantified by defining a mistuning metric as the ratio between the difference in the split frequencies and the center frequency. As verified by substituting Eq. 1 into Eq. 5, the mistuning metric δ is only a function of the vertex-to-vertex distance (a) and the perpendicular width (b):

$$\delta = \frac{2(f_a - f_b)}{f_a + f_b} = \frac{64\sqrt{6}b - 6a}{3a + 32\sqrt{6}b} \tag{5}$$

This means that regardless of boundary conditions and material properties, the mistuning exhibited by a nanowire system is only a function of the geometry of the cross section. Accordingly, the only way to avoid mistuning in such systems is to have a perfectly regular cross section.

For analytical purposes, the nanowire can also be modeled in an approximate sense as a two-degree-of-freedom uncoupled system, as shown in Figure 3. Note that the damping coefficients, C_a and C_b, and the applied forces, F_a and F_b, included here are assumed to be equal (this can be easily generalized where appropriate), and the spring constants, K_a and

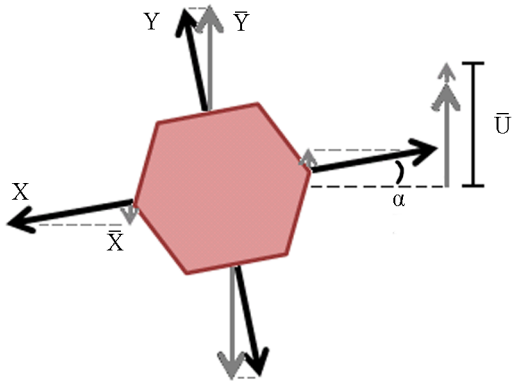

Figure 4: A schematic of the effect of viewing angle on the measured magnitude of the displacement for the two modes.

K_b distinct. This results in a relationship between the natural frequencies and quality factors given by:

$$\frac{f_a}{f_b} = \frac{\omega_a}{\omega_b} = \frac{Q_a}{Q_b} = \frac{(1+\delta/2)}{(1-\delta/2)} \tag{6}$$

Using these relationships as a functional basis, nominal quality factors and natural frequencies for the system can be defined according to:

$$Q = Q_a(1-\delta/2) = Q_b(1+\delta/2) \tag{7}$$

$$\omega_n = \omega_a(1-\delta/2) = \omega_b(1+\delta/2) \tag{8}$$

When the excitation frequency is non-dimensionalized with respect to ω_n, and the two equations of motion are simplified, Eq. 9 and Eq. 10 result:

$$Z_a = \frac{X}{F_b} = \frac{1-(\delta/2)^2}{\omega_n^2(\frac{-r^2}{1-(\delta/2)^2} + \frac{ir}{Q} + \frac{1-\delta/2}{1+\delta/2})} \tag{9}$$

$$Z_b = \frac{Y}{F_a} = \frac{1-(\delta/2)^2}{\omega_n^2(\frac{-r^2}{1-(\delta/2)^2} + \frac{ir}{Q} + \frac{1+\delta/2}{1-\delta/2})} \tag{10}$$

$$r = \frac{\sigma}{\omega_n} \tag{11}$$

In the equations above σ and r are the excitation frequency and normalized excitation frequency, respectively. Note that both equations of motion are identical if there is no mistuning.

In practice, when the system displacement is measured, only the out-of-plane motion can be resolved, so a new variable α is introduced which captures the projection effect due to viewing angle and orientation, as shown in Fig. 4. This renders an observable net displacement given by:

$$\overline{U} = |X\sin\alpha + Y\cos\alpha| \tag{12}$$

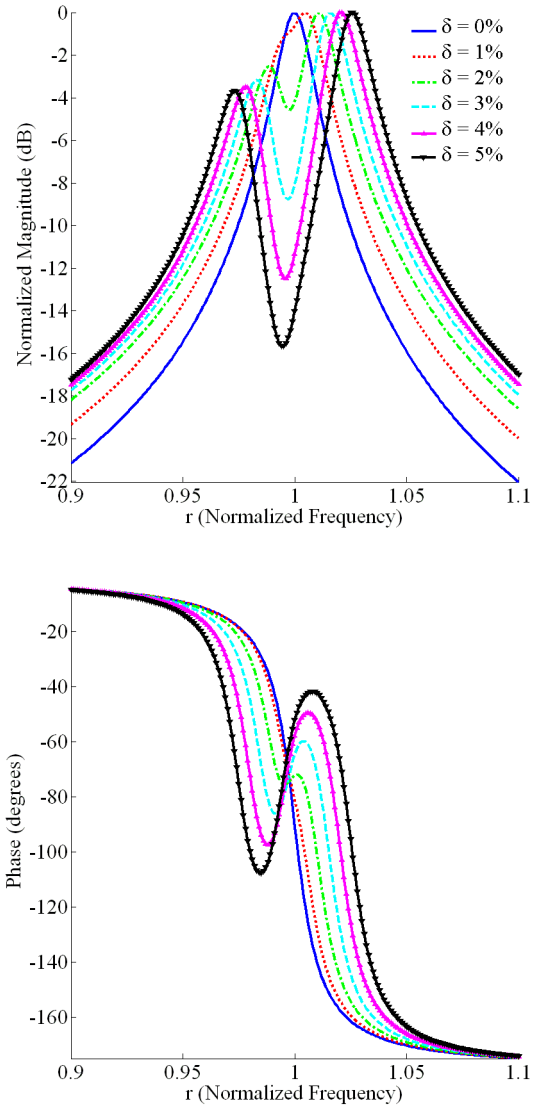

Figure 5: Theoretical frequency response of silicon nanowire as a function of mistuning. Assumed system properties: $Q = 60$, $\alpha = \frac{\pi}{6}$ Radians.

Analysis of this simple model reveals the experimentally-observable effects associated with variations of Q, δ, and α, as succinctly highlighted in Figs. 5-7. Of particular note in these figures is non-Lorentzian nature of the system's response and the fact that the observable quality factor is distorted by the relative proximity of the modes (see Fig. 6). This appears to indicate that conventional Q approximation techniques are insufficient for use with resonant nanosystems with some degree of mode splitting. Also of note is the fact that wire orientation has a dramatic effect on both the quantitative and qualitative nature of the observable response (Fig. 7).

3. Device Fabrication: Silicon nanowires (150 nm in nominal width) were synthesized using the nanocluster-catalyzed vapor-liquid-solid method. In this process, growth is realized through the use of 150 nm gold nanocluster catalysts in conjunction with a silicon reactant (silane), P-type dopant (boron), and hydrogen carrier. Following synthesis, the wires were removed from the growth substrate via sonication and dissolved into isopropyl alcohol. The wires were then deposited by dropper (randomly dispersed) onto a silicon substrate with a 10 μm SU-8 grating pattern. Near field forces were exploited for anchoring. Figure 1 shows a typical nanowire device. Note that since the silicon nanowires examined herein derive from a single fabrication batch, they feature nominally-identical material properties. Accordingly, device-to-device variations in frequency arise solely from varying boundary conditions and length, as well as cross-sectional irregularity.

4. Thermally-Actuated Systems: Following fabrication, a scanning laser Doppler vibrometer was used to measure the thermally-excited displacement response of the nanowire devices in the direction perpendicular to the device substrate, as shown in Figs. 4 and 8. The adopted measurement procedure mirrors that previously used by Biedermann et al. [7] and is akin to that utilized by Belov and collaborators [8]. Samples were measured at room temperature in a 2 mTorr environment. This setting ensured that surface effects and anchor losses were the primary source of dissipation (Q = 30-200) and not molecular-regime fluid damping. Note that the utilized vibrometer could only resolve out-of-plane motions of the thermally-excited system with a noise floor of approximately 150 fm and a resolution of 2 fm. In addition, the planes of vibrations were oriented at an unknown angle with respect to the substrate, due to the random dispersion of the nanowires (as is commonly the case

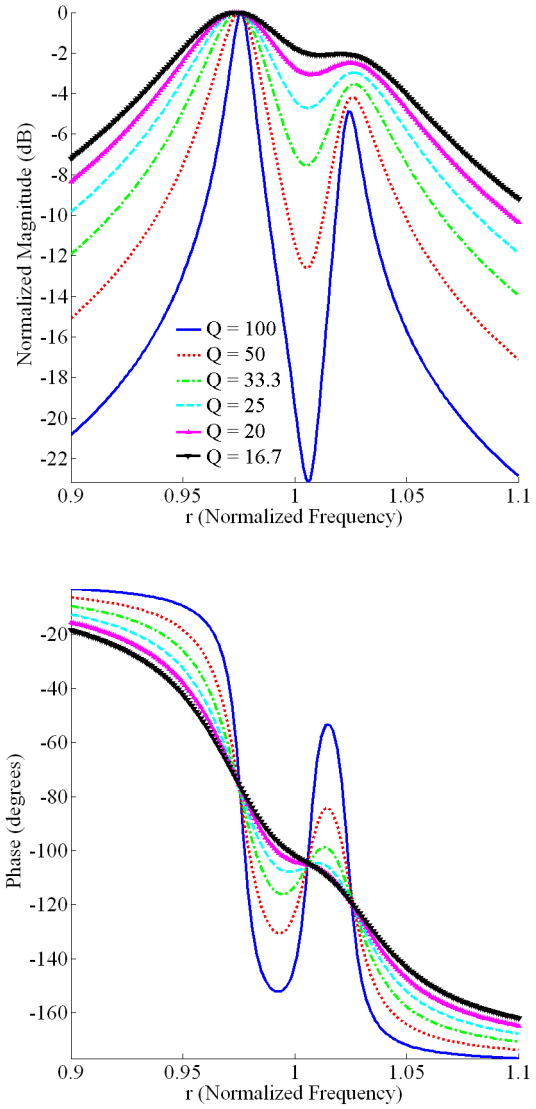

Figure 6: Theoretical frequency response of silicon nanowire as a function of quality factor. Assumed system properties: $\delta = 4.73\%$, $\alpha = \frac{\pi}{6}$ Radians.

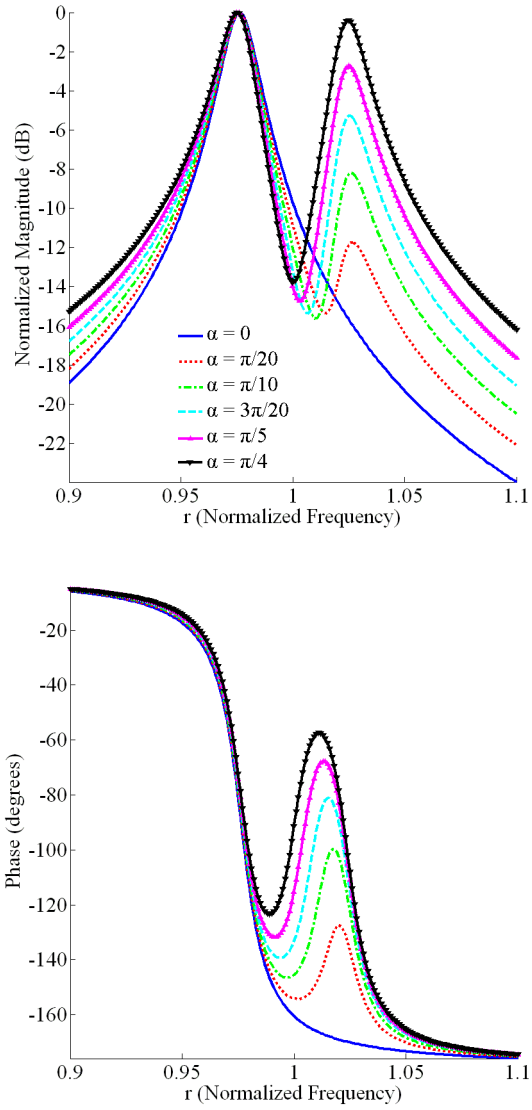

Figure 7: Theoretical frequency response of silicon nanowire as a function of viewing angle. Assumed system properties: $Q = 60$, $\delta = 4.73\%$.

in final device implementations). As a result, the split modes featured orientation-dependent resonant amplitudes, as highlighted in Fig. 2 and Fig. 7.

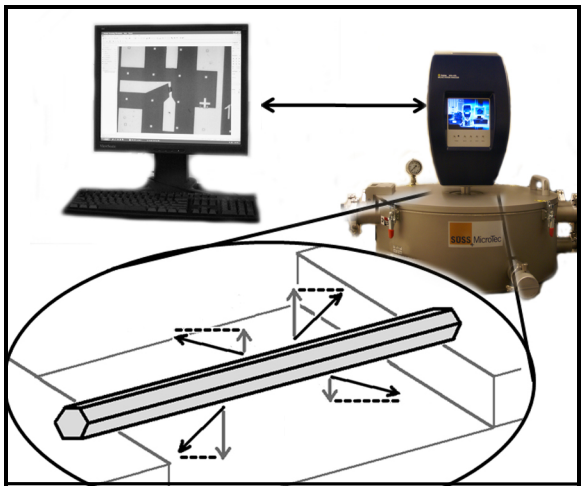

Figure 8: A schematic of the experimental set-up, consisting of a computer-based data acquisition/processing station, Polytec MSA-400 scanning laser Doppler vibrometer, and a Suss Microtec PLV-50 optically-accessible vacuum chamber. Note that the measured displacement is a projection of the device's actual displacement, measured normal to the substrate and is only proportional to the physical response, since the laser's spot size is approximately ten times larger than the nanowires' diameter. In the inset, the black arrows indicate the actual motion of the wire, and the dark grey arrows indicate the measured displacement.

Theory predicts that mode splitting occurs as a function of cross-sectional geometry. Experimental data appears to validate this, in that resonant mode splitting occurred in most of the examined nanowires, regardless of the length of, or boundary conditions associated with, the device (see Table 1). Note that the measured frequencies were all within the geometry-based uncertainty of the theoretical predictions and match within 5%.

The actual mistuning between resonances was extrapolated by substituting the peak frequencies into Eq. 5. The mistuning values that could be calculated from the experimental data ranged from 2% to 10%. A mistuning value of 3% was the most common value of the 13 devices that showed mode splitting. For the cases where no mode splitting was observed either the mistuning was smaller than 2%, resulting in obscured peaks, or the viewing angle was

such that contributions from the second mode were minimal.

Small resonant amplitudes, thermomechanical noise, and a lack of phase information all contributed to the difficulty in matching the analytically-predicted frequency response with experimental results. Despite these issues in some instances it was possible to use nonlinear regression to fit the model presented herein to the experiments. Figure 9 shows the model presented in Eq. 12 plotted with experimental data recovered from a cantilevered nanowire. As evident, there is appreciable fidelity between the simple model and experiment.

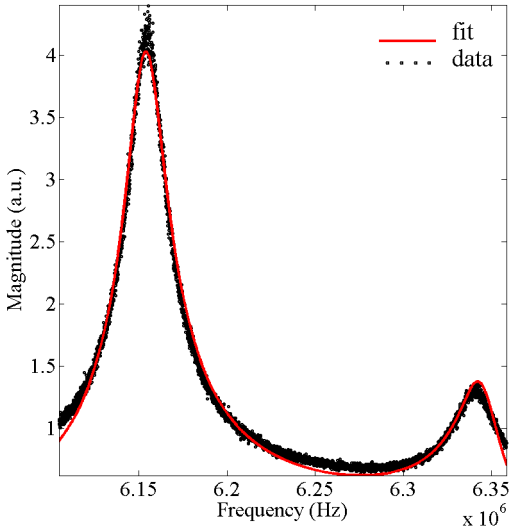

Figure 9: The frequency response of cantilevered device 8 from Table 1 fit with the model presented in Eq. 12. The experimentally-recovered and regression validated center frequency is approximately 6.248 MHz, and the mistuning 3.004%,

5. Electrostatically-Actuated Systems: Though thermal excitation studies are useful for system identification purposes and some device applications, many practical applications require the use of an additional transduction mechanism, typically electrostatic or magnetomotive in nature. Figure 10 shows examples of two electrostatically-actuated nanoresonators currently under development. With these devices it is possible to not only study the effects of cross-sectional asymmetry on coherently-driven systems, but also the impact of noise, nonlinearities, and parametric effects.

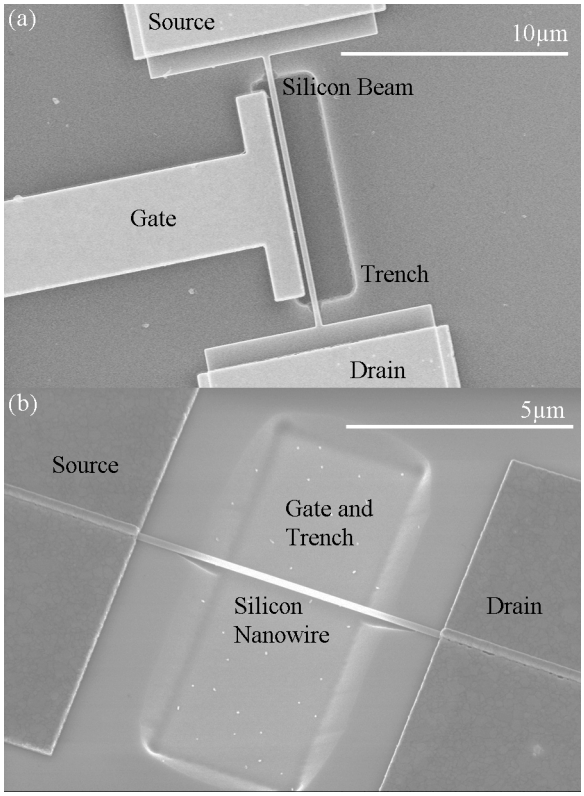

Figure 10: (a) Scanning electron micrograph (SEM) of a silicon-on-insulator (SOI) electrostatically-actuated, side-gate device. (b) SEM of an electrostatically-actuated, bottom-gate device.

6. Conclusions: Mode splitting in silicon nanowire systems occurs due to geometry based irregularities in their cross sections. This effect is independent of material properties and the boundary conditions of the devices, and occurs even when dimensional differences are on the order of 2% of their nominal values. In this paper, the mode splitting was modeled by parameterizing a hexagon, and using a simple two-degree-of-freedom mechanical model to qualitatively and quantitatively capture pertinent dynamics. This modeling approach accurately reflected experimental data in nanowire systems where mode splitting was evident.

Given the simplicity of the systems examined herein, non-Lorentzian frequency responses, akin to those presented here, can be expected in most nanowire devices. Accordingly, designers of functional nanoscale devices, such as resonant mass sensors and electromechanical signal processing elements, should account for this mechanism in the course of device design. For example, in resonant mass sensing applications, device designers should

not only account for added mass and stiffness change effects, but also for quantitative changes in coupling between the split resonant modes. This added complexity should not be seen as a technical deterrent, but rather an opportunity for innovative devices and resonant tuning, as the intentional varying of process parameters should lead to a direct alteration of a given resonator's near-resonant response. Ongoing efforts are aimed at exploiting this opportunity and investigating the effects of cross-sectional asymmetry in the presence of noise, nonlinearity, and/or parametric effects.

7. Acknowledgements: This work was supported by the National Science Foundation under Grant 0826276. The authors would also like to thank W. Zhang, Y. Zhao, and C. Yang of Purdue University for their assistance in preparing the nanowire samples.

8. References:

[1] D. N. Guerra, T. Dunn, and P. Mohanty, *Nano Letters*. **9**, 3096 (2009).

[2] A. K. Naik, M. S. Hanay, W. K. Hiebert, X. L. Feng, and M. L. Roukes, *Nat. Nanotechnol.* **4**, 445 (2009).

[3] X. L. Feng, R. He, P. Yang, and M. L. Roukes, *Nano Letters* **7**, 1953 (2007).

[4] B. Tian, X. Zheng, T.J. Kempa, Y. Fang, N. Yu, G. Yu, J. Huang, and C.M. Lieber, *Nature (London)* **449**, 885 (2007).

[5] E. Gil-Santos, D. Ramos, J. Martìnez, M. Fernàndex-Regùlez, R. Garcìa, À. San Paulo, M. Calleja, and J. Tamayo, *Nat. Nanotechnol.* **5**, 641-5 (2010).

[6] S. L. Garrett, *J. Acoust. Soc. Am.* **88**, 210 (1990).

[7] L. B. Biedermann, R. C. Tung, A. Raman, and R. G. Reifenberger, *Nanotechnology* **20**, 035702 (2009).

[8] M. Belov, N. J. Quitoriano, S. Sharma, W. K. Hiebert, T. I. Kamins, and S. Evoy, *J. Appl. Phys.* **103**, 074304 (2008).

Table 1: Theoretical and experimental natural frequencies of the silicon nanowires. Assumed material and geometric properties: $\rho = 2339$ kg/m^3, $E = 189$ GPa, $a = 159$ nm, and $b = 148$ nm. Quality factors were large enough to allow for direct comparison between undamped theory and the experiment (for the number of significant digits shown). Also note that C = cantilevered; FP = fixed-pinned; and FF = fixed-fixed boundary conditions. Finally, stars in the mistuning column indicate systems where splitting was present but the second frequency could not be recovered.

Boundary Conditions	**Length (μm)**	**Undamped Theory (MHz)**		**Experiment (MHz)**		**δ (%)**
C1 M1	8.42	2.61 ± 0.17	2.74 ± 0.19	2.47	2.60	4.934
C1 M2	8.42	16.36 ± 1.09	17.16 ± 1.17	16.31	–	–
C2	6.92	3.87 ± 0.30	4.05 ± 0.32	–	3.98	–
C3	7.39	3.39 ± 0.25	3.55 ± 0.27	3.11	–	$*$
C4	6.81	3.99 ± 0.32	4.18 ± 0.34	3.77	3.90	3.372
C5	5.66	5.78 ± 0.54	6.06 ± 0.58	5.68	5.82	2.435
C6	5.43	6.28 ± 0.61	6.58 ± 0.63	6.15	6.34	3.004
C7	4.93	7.62 ± 0.81	7.99 ± 0.83	6.84	7.32	6.853
FP1	8.92	10.12 ± 0.65	10.69 ± 0.70	–	10.61	–
FP2	9.59	8.82 ± 0.53	9.25 ± 0.57	8.46	9.14	7.765
FP3	9.21	9.57 ± 0.60	10.03 ± 0.64	–	10.56	–
FP4	9.76	8.52 ± 0.51	8.93 ± 0.55	8.27	9.14	9.960
FF1	11.33	8.95 ± 0.48	9.62 ± 0.53	9.09	9.39	3.215
FF2	10.40	10.89 ± 0.62	11.42 ± 0.67	10.47	10.80	3.103
FF3	9.41	13.30 ± 0.82	13.95 ± 0.88	14.60	15.11	3.456
FF4	10.55	10.58 ± 0.60	11.10 ± 0.65	–	12.15	–
FF5	13.07	6.90 ± 0.34	7.23 ± 0.37	6.79	7.17	5.305
FF6	9.73	12.44 ± 0.74	13.05 ± 0.80	12.50	–	–
FF7	9.76	12.37 ± 0.74	12.97 ± 0.80	11.86	–	–
FF8	10.05	11.66 ± 0.68	12.23 ± 0.73	–	12.85	–
FF9	10.24	11.23 ± 0.65	11.78 ± 0.70	–	12.08	–
FF10	9.12	14.16 ± 0.89	14.85 ± 0.96	14.46	14.68	1.556
FF11	10.33	11.04 ± 0.63	11.57 ± 0.68	–	12.10	$*$
FF12	10.35	11.00 ± 0.63	11.53 ± 0.68	–	11.80	–